Anisotropic Polyoxometalate Cages Assembled via Layers of Heteroanion Templates
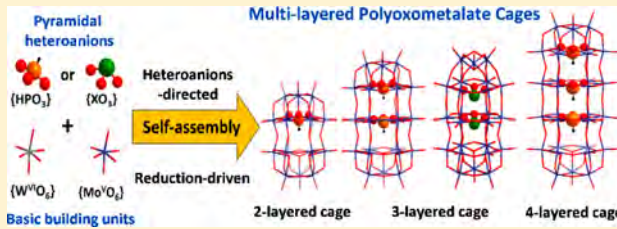
Qi Zheng,[†] Manuel Kupper,[†] Weimin Xuan,[†] Hirofumi Oki,[‡] Ryo Tsunashima,[‡] De-Liang Long,*,[†] and Leroy Cronin*,[†]

[†]School of Chemistry, The University of Glasgow, Glasgow G12 8QQ, U.K.
[‡]Graduate School of Sciences and Technology for Innovation, Yamaguchi University, Yoshida 1677-1, Yamaguchi 753-8512, Japan

Ⓢ *Supporting Information*

ABSTRACT: The synthesis of anisotropic redox-active polyoxometalates (POMs) that can switch between multiple states is critical for understanding the mechanism of assembly of structures with a high aspect ratio, as well as for their application in electronic devices. However, a synthetic methodology for the controlled growth of such clusters is lacking. Here we describe a strategy, using the heteroanion-directed assembly, to produce a family of 10 multi-layered, anisotropic POM cages templated by redox-active pyramidal heteroanions with the composition $[W_{16}Mo_2O_{54}(XO_3)]^{n-}$, $[W_{21}Mo_3O_{75/76}(XO_3)_2]^{m-}$, and $[W_{26}Mo_4O_{93}(XO_3)_3]^{o-}$ for the double, triple, and quadruple layered clusters, respectively. It was found that the introduction of reduced molybdate is essential for self-assembly and results in mixed-metal (W/Mo) and mixed-valence (W^{VI}/Mo^V) POM cages, as confirmed by an array of analytical techniques. To probe the archetype in detail, a tetrabutyl ammonium (TBA) salt derivative of a fully oxidized two-layered cage is produced as a model structure to confirm that all the cages are a statistical mixture of isostructures with variable ratios of W/Mo. Finally, it was found that multilayered POM cages exhibit dipolar relaxations due to the presence of the mixed valence W^{VI}/Mo^V metal centers, demonstrating their potential use for electronic materials.

INTRODUCTION

Polyoxometalates (POMs) are a unique class of discrete molecular metal-oxides with a diversity of structures and properties.[1−4] Studies of POMs are important for exploring assembly processes at the molecular level, as well as for the development of new redox-active devices.[5−10] As an important subclass, heteropolyoxometalates (HPOMs), generally templated by heteroanions (HAs) with a variety of geometries, have attracted wide attention in recent years owing to their structural diversity and stability, rich electrochemistry, and appealing catalytic activities.[11−13] In particular, the incorporation of pyramidal redox-active HAs into HPOMs not only leads to the discovery of a series of unconventional Dawson-type HPOMs but also allows the facile tuning of redox properties arising from the intramolecular electronic interactions between encapsulated HAs and the metal oxide framework.[14,15] To date, pyramidal $[XO_3]^{2-}$ HAs have been successfully incorporated into "peanut"-shaped Dawson-like clusters $[M_{18}O_{54}(XO_3)_n]^{4-/8-}$ (n = 1, 2; X = As, Bi, S, Se, HP, etc.) and "Trojan-horse"-type clusters $[W_{18}O_{56}(XO_3)_2(H_2O)_2]^{8-}$ (X = S, Se or HP).[9,16−22] The oxidation of redox-active HAs can be coupled with the reversible multielectron transfer to the metal oxide shells of HPOMs, allowing switching of the electronic state, and this has been used to construct a flash memory architecture.[9] As such, it would be of interest to further develop HPOM cages, especially those comprising multiple layers incorporating a
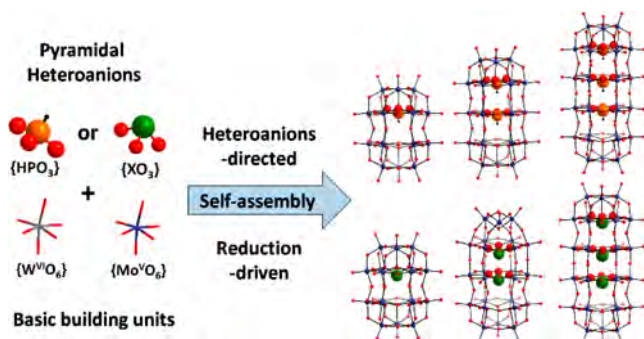
number of HAs, beyond $\{M_{30}O_{90}\}$ (M = W or Mo) incorporating both pyrophosphate and HPO_3^{2-}.[23−26]

Herein, we present a strategy to produce multilayered cylinder-type HPOMs by introducing reduced Mo as a heterometal, resulting in a family of mixed-metal and mixed-valence (W^{VI}/Mo^V) POM clusters, templated by $[XO_3]^{2-}$ (X = HP, Se, Te) HAs (Scheme 1). This work was inspired by the reduction-driven formation of giant molybdenum blue (MB) clusters, including wheel-shaped $\{Mo_{154}\}$, $\{Mo_{176}\}$, blue "lemon" $\{Mo_{368}\}$, as well as molybdenum brown sphere $\{Mo_{132}\}$[27−32] and its mixed-metal analogue $\{W^{VI}_{72}Mo^V_{60}\}$.[33,34] All ten compounds **1−11** obtained here exhibit cylinder cage-like frameworks consisting of 2−4 metal layers and 1−3 HAs. Compounds **1−3** share the same two-layered peanut-shaped framework, templated by three types of HAs, respectively. Compounds **4−6** feature unprecedented three-layered cage structures, while **7** and **8** exhibit unique three-layered cages, templated by mixed HAs. Compounds **9** and **10** present four-layered cage structures and are constructed solely from pyramidal HAs. Compound **11** is the cation-exchanged, TBA salt, derivative of **3** in its fully oxidized state. All compounds were characterized crystallographically, and the formula assignments are supported by an extensive array of analytical techniques (see the Supporting Information).

Scheme 1. Schematic Representation of Pyramidal Heteroanion-Directed and Reduced Mo^V-Driven Assembly of Multilayered POM Cages[a]

[a]Color scheme: P, orange; $\{XO_3\}$ (X = Se, Te), green; W/Mo^V, indigo; O, red; H, black.

RESULTS AND DISCUSSION

Synthesis of 1−11. $[Mo_2O_4(H_2O)_2]^{2+}$ was used as a source of reduced Mo in the well-established synthetic reaction for pyramidal HA-templated POM cages (see Experimental Section for details).[35] Dark blue crystals $(C_2H_8N)_7H_3[W^{VI}_{16}Mo^V_2O_{57}(HPO_3)]\cdot10H_2O$ (1), $(C_2H_8N)_7H_3[W^{VI}_{16}Mo^V_2O_{57}(SeO_3)]\cdot10H_2O$ (2), and $(C_2H_8N)_7H_3[W^{VI}_{16}Mo^V_2O_{57}(TeO_3)]\cdot10H_2O$ (3) were obtained from a reaction containing $Na_2WO_4\cdot2H_2O$, dimethylamine hydrochloride (DMA·HCl), $[Mo_2O_4(H_2O)_2]^{2+}$, and $[XO_3]^{2-}$ (X = HP, Se, Te) at 50 °C. Under more dilute conditions, decreasing the ratio of $[WO_4]^{2-}/[XO_3]^{2-}$ led to the formation of three-layered cage structures $(C_2H_8N)_{11}NaH[W^{VI}_{21}Mo^V_3O_{75}(HPO_3)_2]\cdot15H_2O$ (4), $(C_2H_8N)_{11}NaH_3[W^{VI}_{21}Mo^V_3O_{76}(SeO_3)_2]\cdot14H_2O$ (5), and $(C_2H_8N)_{10}NaH_3[W^{VI}_{22}Mo^V_2O_{76}(TeO_3)_2]\cdot14H_2O$ (6). To further explore and understand the influence of HAs on the self-assembly of multilayered POM clusters, mixed HAs of $[HPO_3]^{2-}/[SeO_3]^{2-}$ or $[HPO_3]^{2-}/[TeO_3]^{2-}$ were introduced into the synthesis under the same reaction conditions of 4−6, resulting in two three-layered analogues $(C_2H_8N)_{10}NaH[W^{VI}_{22}Mo^V_2O_{75}(HPO_3)(SeO_3)]\cdot15H_2O$ (7) and $(C_2H_8N)_{11}NaH[W^{VI}_{21}Mo^V_3O_{75}(HPO_3)(TeO_3)]\cdot15H_2O$ (8), respectively. Under the same synthetic conditions as used for the synthesis of 4, a slight increase of the temperature from 50 to 65 °C led to the generation of a four-layered cluster $(C_2H_8N)_{16}[W^{VI}_{26}Mo^V_4O_{93}(HPO_3)_3]\cdot15H_2O$ (9) as a side product of 4. Replacing $[HPO_3]^{2-}$ with $[SeO_3]^{2-}$ in the synthesis reaction for 9 afforded $(C_2H_8N)_{30}NaH$-$[W^{VI}_{26}Mo^V_4O_{93}(SeO_3)_3][W^{VI}_{36}O_{112}(SeO_3)_4]\cdot40H_2O$ (10). Finally, exchanging the DMA in compound 3 with tetrabutylammonium (TBA) resulted in the isolation of fully oxidized colorless $(C_{16}H_{36}N)_5[H_3TeW^{VI}_{16}Mo^{VI}_2O_{60}]$ (11).

Crystal Structures of 1−11. Single-crystal X-ray structure analysis reveals that 1−3 share the same peanut-shaped framework of the previously reported single pyramidal HA-containing $\{W_{18}O_{54}(XO_3)\}$ (X = Bi, As, S),[17−21] which consists of two equal $\{M_9O_{30}\}$ (M = W/Mo) moieties linked by six oxo ligands (Figure 1a,b), showing a distinct difference from the Trojan-horse-type $[W_{18}O_{56}(XO_3)_2(H_2O)_2]^{8-}$ (Figure 1c).[16,22] Compared with these clusters, the novelty of compounds 1−3 arises from the reduced cage shell consisting of mixed Mo^V/W^{VI} metal sites, as confirmed by their characteristic blue color, derived from intervalence charge
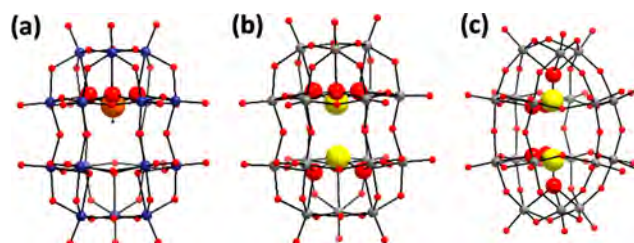

Figure 1. Structural representations of (a) $[W^{VI}_{16}Mo^V_2O_{57}(XO_3)]^{10-}$ (X = HP for 1, X = Se for 2, X = Te for 3). (b) Peanut-shaped cluster $[X_2W_{18}O_{60}]^{4-}$ (X = S, Se). (c) "Trojan-horse" type clusters $[W_{18}O_{56}(XO_3)_2(H_2O)_2]^{8-}$ (X = S, Se, HP). Color scheme: P or Se or Te, orange; S, yellow; W/Mo^V, indigo; W, gray; O, red.

transfer between the mixed-valence metal sites, as well as by elemental analysis (see the Supporting Information for details). In compounds 1−3, one HAs $[HPO_3]^{2-}$, $[SeO_3]^{2-}$ or $[TeO_3]^{2-}$ is enclosed in the cluster. The heteroatom P, Se or Te is disordered over two positions with half occupancy on each position, which deviates ~1.61, ~ 1.50 and ~1.27 Å from the cluster center, respectively (Figure 1a). A similar phenomenon has also been found in the reported $\{W_{18}O_{54}(XO_3)_2\}$ (X = Bi, As, etc.) analogues.[17−21]

Compound 4 can be regarded as a novel extended peanut-shaped cage, by effectively inserting an additional layer of $\{M_6O_{18}(HPO_3)\}$ (M = W/Mo) into the middle of compound 1 (Figure 2 and Figure S1). The two $[HPO_3]^{2-}$ HAs, located

Figure 2. Structural representations of pyramidal heteroanion-controlled assembly of extended three-layered peanut-shaped cages 4, 7, and 8 and bullet-shaped cages 5 and 6, where X = Se or Te. Color scheme: P, orange; Se, green; Te, purple; W/Mo^V, indigo; O, red; H, black.

in the middle and top layers, display an eclipsed arrangement with respect to one another. Interestingly, in contrast to all known cylinder-shaped POM cage clusters, compound 5 and 6 are neither olive-shaped nor peanut-shaped, but an unprecedented bullet-shaped structure with a pointed top and flat bottom (Figure 2). Overall, the molecular structures of 5 and 6 can be considered as an integrated cluster built from a $\{M_{15}(XO_3)_2\}$ (X = Se or Te) unit in an olive-shaped Dawson and a $\{M_9\}$ unit in a peanut-shaped Dawson. Because of the size restriction within 5 and 6, only two HAs are located on the

two belts near the pointed end, in an eclipsed arrangement, leaving the belt near the bottom end empty. It should be noted that compounds **4**−**6** represent the first examples of three-layered cage-like POM clusters containing multiple HAs; their discovery greatly diversifies the structural library of Dawson-type clusters. More importantly, the presence of both olive-shaped and peanut-shaped Dawson fragments in one molecule (**5** and **6**) shows the potential to build novel multilayered clusters based on controlled aggregation of these building blocks. Moreover, the formation of **5** and **6** under the same conditions as **4** implies the electronic nature and size of the HAs also play an important role in directing the assembly of the resultant clusters.

Structure determination reveals **7** and **8** share the same framework as **4**, in which $[HPO_3]^{2-}$ is always located at the center of the middle belt while the larger $[SeO_3]^{2-}$ or $[TeO_3]^{2-}$ are disordered equally at the two ends, each with half occupancy (Figures 2 and S2). Because of the distinctly different electronic properties and relative sizes between the two mixed HAs, the HAs can be fully differentiated and identified in two well-defined positions via self-sorting, a principle which has already been observed in the assembly of cross-shaped POM clusters $[(XYW_{15}O_{54})_4(WO_2)_4]^{32-/36-}$ (X = HP, Y = Se, Te, As).[36] This arrangement results from the approximately tetrahedral configuration adopted by $[HPO_3]^{2-}$, which requires more space for its accommodation compared with pyramidal-shaped $[SeO_3]^{2-}$ or $[TeO_3]^{2-}$ and thus preferentially occupies the middle of the structure while keeping one end occupied by another type of HA. The same arrangement has also been observed in the cross-shaped POM clusters where the smaller $[HPO_3]^{2-}$ occupies the uncapped end. On the basis of the crystal structures of **4**−**8**, it can be concluded that the architectures of three-layered POM clusters are directly regulated by the selected HAs. The smaller $[HPO_3]^{2-}$ always favors the formation of extended peanut-like cages, even in the presence of another type of pyramidal HA, while larger $[XO_3]^{2-}$ (X = Se, Te) facilitates the assembly of solely bullet-shaped clusters (Figure 2).

The successful isolation of a series of three-layered POM cages encouraged us to further extend multilayered clusters. Compound **9** also shows an extended peanut-shaped cage structure but with four belt layers capped by two $\{M_3O_6\}$ triads (Figures 3 and S3). In this context, the shell of **9** could
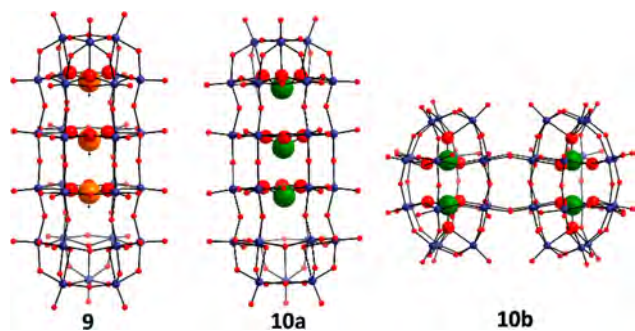

Figure 3. Structural representations of $[HPO_3]^{2-}$ templated four-layered cage structure $[W^{VI}_{26}Mo^{V}_4O_{93}(HPO_3)_3]^{16-}$ (**9**) and $[SeO_3]^{2-}$ templated cluster **10** consisting of a four-layered $[W^{VI}_{26}Mo^{V}_4O_{93}(SeO_3)_3]^{16-}$ (**10a**) cocrystallized with a dimeric "Trojan-horse" type cluster $[W_{36}O_{112}(SeO_3)_4]^{16-}$ (**10b**). Color scheme: HP, orange; Se, green; W^{VI}/Mo^{V}, indigo; O, red; hydrogen, black.

be regarded as a fusion of lacunary $\{M_{15}O_{39}(HPO_3)_2\}$ and $\{M_{15}O_{39}(HPO_3)\}$ (M = W/Mo) moieties. In total there are three $[HPO_3]^{2-}$ encapsulated in **9**, which are disordered evenly on the consecutive three belts from either end. Although four-layered POM cages $\{M_{30}O_{90}(P_2O_7)_n(XO_3)_m\}$ (M = W, Mo; X = HP, Se; n = 1, 2; m = 2, 0) have been reported by adopting either pyrophosphate or a mixture of pyrophosphate and pyramidal $\{XO_3\}$ as templates,[23−26] we demonstrate here for the first time that four-layered cages can be constructed from a single type of $\{XO_3\}$, which not only represents a key step toward the versatile synthesis of $\{XO_3\}$-templated multilayered clusters but also realizes our previous hypothesis to build four-layered HPOMs based on unconventional HAs.[37]

Compound **10** consists of a four-layered $[Se_3W_{26}Mo_4O_{102}]^{16-}$ (**10a**) cocrystallized with a dimeric cluster $[Se_4W_{36}O_{124}]^{16-}$ (**10b**). **10a** is isostructural to the cluster in **9** but with three $[SeO_3]^{2-}$ anions distributed over the three belt layers (Figures 3 and S4). **10b** is observed for the first time and features a dimeric motif constructed from two Trojan-horse $[W_{18}O_{56}(SeO_3)_2(H_2O)_2]^{8-}$ ($\{Se_2W_{18}\}$) clusters by removing water ligands and linking up along these water ligand sites (Figure 3).[9] The presence of both peanut-shaped and Trojan-horse clusters in **10** indicate the competitive formation of these clusters during the self-assembly. Indeed, Trojan-horse $\{Se_2W_{18}\}$ was the predominant product after the reaction, and compound **10** can be obtained only after the formation of $\{Se_2W_{18}\}$. Upon removal of the crystals of $\{Se_2W_{18}\}$ over several instances, dark blue **10** started to appear in the solution with relatively low yield. Compound **11** is isostructural to compound **3** and could be considered as a fully oxidized and TBA-exchanged derivative with the two Mo centers in $[H_3TeW^{VI}_{16}Mo^{VI}_2]^{5-}$ adopting +6 valence.

Reduced States of 1−10 and the Critical Role of Reduced Agents during Self-Assembly. All the compounds **1**−**10** display broad absorption bands at around 550 and 850 nm in the UV−vis−NIR spectra due to heteronuclear charge transitions $Mo^{5+} \rightarrow W^{6+}$ (see Figure S5).[38,39] Because molybdenum centers are much easier to reduce than tungsten and can preserve the reduced clusters in both solution and solid phase, we considered that all the Mo sites retain the original valence of +5 from $[Mo_2O_4(H_2O)_2]^{2+}$, whereas all the W centers adopt +6 oxidation state. Also, redox titrations further confirmed that clusters **1**−**10** were reduced between 2 and 4 electrons, which is consistent with the ICP-OES data (see the Supporting Information). It is worth noting that the presence of reduced Mo species is essential to induce the formation of multilayered clusters **4**−**10**. Control experiments showed that only tungsten-based Trojan-horse or peanut type $\{W_{18}\}$ clusters formed when replacing $[Mo_2O_4(H_2O)_2]^{2+}$ with fully oxidized $[MoO_4]^{2-}$ in the synthesis of **4**−**10**. In contrast, addition of reducing agents such as hydrazine to the solution containing $[WO_4]^{2-}$ and $[MoO_4]^{2-}$ led to the isolation of multilayered structures in a manner similar to $[Mo_2O_4(H_2O)_2]^{2+}$ (details in Scheme S1). Mixing reducing agents with $[WO_4]^{2-}$ under the same conditions, however, did not afford the targeted clusters but Trojan-horse or peanut type $\{W_{18}\}$. These results clearly illustrate the key role of reduced Mo species in directing the self-assembly of multilayered POM clusters and support our assumption that all the reduced electrons are located on Mo centers. Although three-layered $\{W_{21}(TeO_3)_3\}$ has been reported as a pure tungsten-based cluster, it features only an open cage-like structure with one end free of a cap.[36] It seems that the

incorporation of the Mo^V ions can cause the slight changes in the curvature of the cluster skeleton, which is usually observed in Molybdenum Blues[27−30] and will facilitate the formation of closed cage-like structures $1−10$. Moreover, the elemental analysis of compounds $1−10$ indicated that the addition of one layer in the cluster will roughly account for the increase of one Mo^V ion. The structural driving force for this may arise from the different ion radius between Mo^V and W^{VI}. Because $Mo^V−O$ length is slightly shorter than $W^{VI}−O$, the amount of Mo^V within one $\{W_{6−x}Mo_x\}$ layer should in principle not exceed one in order to accommodate large heteroatoms such as Se and Te. Otherwise, if more Mo^V ions are incorporated, the $\{W_{6−x}Mo_x\}$ layer becomes too small to accommodate the heteroatoms.

Determination of the Compositions of 1−11. Because of the similar structural preferences for Mo and W, both atom types can, in principle, occupy the same metal site anywhere on the cluster shells of compounds $1−10$. Therefore, it is impossible to determine the exact sites of Mo and the ratio of Mo:W from crystal structure determinations because of mixed-metal disorder. The current ratio of Mo:W presented in the formulas is deduced from ICP-OES analysis, which corresponds to the average composition representing a statistical combination of all possible compositions of W and Mo in the structures, as is evidenced by ESI-MS analysis of 1−3 (see Figures S6−S8 and Tables S5−S7 for specific assignments).[40] In order to further confirm the variable composition of W and Mo in one cluster, the tetrabutylammonium (TBA)-exchanged and fully oxidized $(C_{16}H_{36}N)_5[H_3TeW^{VI}_{16}Mo^{VI}_2]$ (11) was selected for MS and NMR studies. In general, the TBA exchanged cluster analogue gives much better mass spectra from the organic phase than the pristine cluster in water. Additionally, it is difficult to obtain high-resolution NMR spectra for the reduced clusters, and therefore, the nonreduced cluster 11 is a good candidate for NMR study. As seen in the ESI-MS spectrum of compound 11 (Figure S10), the intact molecular species were observed in charge states ranging from −4 to −3 with different compositions varying from $\{TeW_{17}Mo_1O_{60}\}$ to $\{TeW_{13}Mo_5O_{60}\}$ (see Table S8), i.e. m/z 1599.0 for $[(TeW_{17}Mo_1O_{60})(TBA)_2H_3]^{3−}$, 1570.0 for $[(TeW_{16}Mo_2O_{60})(TBA)_2H_3]^{3−}$, 1539.9 for $[(TeW_{15}Mo_3O_{60})(TBA)_2H_3]^{3−}$, 1511.9 for $[(TeW_{14}Mo_4O_{60})(TBA)_2H_3]^{3−}$, and 1482.9 for $[(TeW_{13}Mo_5O_{60})(TBA)_2H_3]^{3−}$. This is further verified by NMR studies. As shown in Figure S10, the ^{125}Te NMR spectrum of compound 11 exhibits multiple peaks in the region of 1769−1779 ppm. The presence of multiple peaks with similar chemical shifts indicates that a mixture of $\{W_{18−x}Mo_x(TeO_3)\}$ clusters with varying Mo/W ratios coexist in the solution, as only one singlet should be observed for a pure cluster with specific composition, which is the case of cross-shaped $[W_{64}O_{220}(HPO_3)_4(TeO_3)_4]^{32−}$.[36]

Dielectric Measurements of Anisotropic Cages. To explore the electrical properties of the cluster, temperature-dependent dielectric measurements for compounds 3, 4, and 6 were studied. The inspiration for this study was the fact that a mixed-valence Keggin $[PMo^V_2Mo^{VI}_{10}O_{40}]^{5−}$ was reported to exhibit dielectric relaxation around 50−120 K that was correlated to the mixed-valence states.[41] A similar anomaly was not observed for isostructural but fully oxidized $[BW^{VI}_{12}O_{40}]^{5−}$. Dipole relaxation was evident to originate from the mixed-valence state. Taking the relaxation time scale of electron hopping rate in the POMs (usually faster than 10^8

$s^{−1}$) into account, dipole relaxation cannot be explained by only a hopping process of the electrons, but rather suggests charge relaxation from a disproportionated structure to a fully delocalized structure. Indeed, these compounds showed a similar Debye-type relaxation at 50−150 K (Figures 4, S11,
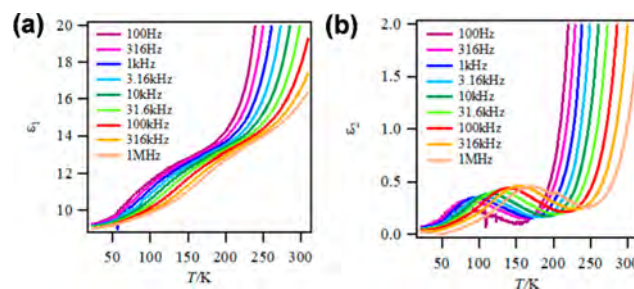

Figure 4. Temperature dependence of (a) real ε_1 and (b) imaginary ε_2 parts of the complex dielectric constant for 3, characterized by the impedance method in the frequency range from 100 Hz to 1 MHz.

and S12). By fitting the Arrhenius equations with temperature and frequency for a peak of ε_2, activation energies of relaxation were estimated to be 0.13, 0.15, and 0.10 eV for 3, 4, and 6, respectively (Figure S13 and Tables S9−S11). These values are relatively lower than that expected for proton conduction by crystalline water.[42] Thermal motion by cation also requires higher activation energy than proton hopping. The ε_1 value reached $10^1−10^2$ upon heating to room temperature. Such a large value is indicative of enriched thermal motion of cations and proton conduction. It was deduced that rapid dipole relaxations observed around 50−150 K are due to the mixed-valence system in the multilayered POM cages, demonstrating their potential use for electronic devices.

■ CONCLUSIONS

In summary, we describe the heteroanion-directed and reduction-driven assembly of a series of multilayered POM cages $1−10$ templated by 1−3 redox-active pyramidal HAs. Compounds $1−3$ share the same two-layered peanut-shaped framework of $\{W_{18}O_{54}(XO_3)\}$ templated by one HA. Under more diluted conditions, decreasing the ratio of $[WO_4]^{2−}/[XO_3]^{2−}$ led to the formation of three-layered cage structures $4−8$ that feature either unprecedented extended peanut-shaped or bullet-shaped cage structures, regulated by the HAs. This not only renews and expands the structural library of HPOM clusters but also emphasizes the key role of HAs in the self-assembly. A slight increase in the reaction temperature led to the generation of four-layered clusters 9 and 10, which show four-layered cage structures, but constructed solely from three pyramidal HAs. Control experiments indicated reduced Mo is essential for the self-assembly of multilayered POM cages $4−10$, and the presence of reduced Mo^V and variable compositions of W and Mo in $1−10$ were confirmed by UV−vis−NIR, NMR spectroscopy, and mass spectrometry. Moreover, the ESI-MS and NMR study of the nonreduced 11 further confirmed the variable composition of W and Mo in $1−10$. Finally, the presence of reduced Mo^V centers was exploited not only in the assembly of the structures but also in the measurement of the dipole relaxations in the multilayered POM. These relaxation parameters demonstrate their potential use for electronic devices. Future work will look to increase the layer numbers even further with the aim of producing molecules with very large aspect ratios.

■ EXPERIMENTAL SECTION

Materials and Instrumentation. All reagents and solvents were purchased from commercial sources and used as received. Elemental analyses (Mo, W, Na, P, Se and Te) were performed via ICP-OES. C, H, and N contents were determined by microanalysis using an EA 1110 CHNS, CE-440 Elemental Analyzer. Thermogravimetric analysis was performed on a TA Instruments Q 500 Thermogravimetric Analyzer under nitrogen flow at a typical heating rate of 10 °C min^{-1}. UV–vis–NIR spectra were collected using a SPECORD S600 Analytic Jena spectrophotometer in transmission mode using quartz cuvettes with a 1.0 cm optical path length. Infrared spectra (4000–400 cm^{-1}) of all samples were recorded on a JASCO FTIR-410 spectrometer or a JASCO FT-IR 4100 spectrometer. ^{125}Te NMR spectroscopy were recorded on a Bruker AVIII 600 MHz spectrometer. All MS data was collected using a Qtrap, time-of-flight MS (Maxis Impact) instrument supplied by Bruker Daltonics Ltd. Temperature-dependent dielectric permittivity was measured using an Agilent E4980A Precision LCR meter.

X-ray Crystal Structure Analysis. Suitable single crystals were selected and mounted by using the MiTeGen MicroMounts kit with Fomblin oil. X-ray diffraction intensity data were measured at 150(2) K on a Bruker Apex II Quazar diffractometer using Mo Kα radiation [λ = 0.71073 Å]. Structure solution and refinement were carried out with SHELXS[43] and SHELXL-2014[44] via WinGX.[45] Corrections for incident and diffracted beam absorption effects were applied using empirical methods.[46] The X-ray crystallographic data for structures reported in this article have been deposited at the Cambridge Crystallographic Data Centre, under deposition numbers CCDC 1885487−1885496.

Preparation of $[Mo^V_2O_4(H_2O)_2]^{2+}$ in 4 M HCl ({Mo$_2$}). The synthesis is based on a reported procedure.[35] Hydrazine monohydrate (64–65%, 840 µL) was added to a suspension of 9.2 g molybdenum trioxide in 320 mL of 4 M HCl. The solution was heated at 60 °C for 3 h.

Synthesis of (C$_2$H$_8$N)$_7$H$_3$[HPW$_{16}$Mo$_2$O$_{60}$]·10H$_2$O (1). Sodium tungstate dihydrate (2.5 g, 7.6 mmol), phosphorous acid (0.04 g, 0.48 mmol), and dimethylamine hydrochloride (DMA·HCl) (1.2 g, 14.7 mmol) were dissolved in 20 mL of water. Around 2.8 mL of {Mo$_2$} was added dropwise under stirring, and the solution pH consequently reached 2.2. The solution was heated with stirring at around 50 °C for 30 min. Upon cooling to room temperature, a dark blue powder formed and was removed by filtration. Dark blue block crystals were isolated from the filtrate after a few days. These crystals were collected by soaking the solid using filtered mother liquor to remove further blue powder (Yield: 8.3% based on W). Characteristic IR bands (cm^{-1}): 3419(b), 3151(b), 2980(s), 2785(w), 2451(w), 1614(m), 1462(s), 1379(m), 1249(w), 1153(w), 1066(m), 951(s), 721(s), 501(w). Elemental analysis for C$_{14}$H$_{80}$N$_7$P$_1$W$_{16}$Mo$_2$O$_{70}$, M_W = 4631.23 g mol^{-1}, calc (%): W 63.51, Mo 4.14, P 0.67, H 1.74, C 3.63, N 2.11; found (%): W 64.09, Mo 3.87, P 0.76, H 1.63, C 3.14, N 2.32. Calculated TGA water loss from 25 to 200 °C (%): calculated, 3.9; found 3.1.

Synthesis of (C$_2$H$_8$N)$_7$H$_3$[SeW$_{16}$Mo$_2$O$_{60}$]·10H$_2$O (2). Sodium tungstate dihydrate (2.5 g, 7.6 mmol), sodium selenite (0.08 g, 0.46 mmol), and dimethylamine hydrochloride (DMA·HCl) (1.2 g, 14.7 mmol) were dissolved in 20 mL of water. {Mo$_2$} (2.8−3.4 mL) was added dropwise under stirring, and the solution pH consequently reached 1.3−2.6. The solution was heated with stirring at around 50 °C for 30 min. Upon cooling to room temperature, a dark blue powder formed and was removed by filtration. Dark blue block crystals were isolated from the filtrate after 1 week. These crystals were collected by soaking the solid using filtered mother liquor to remove further blue powder (Yield: 22.4% based on W). Characteristic IR bands (cm^{-1}): 3452(b), 3140(b), 2980(s), 2779(m), 2453(w), 1614(m), 1462(s), 1388(m), 1253(w), 1161(s), 1068(m), 1018(m), 950(s), 704(s). Elemental analysis for C$_{14}$H$_{79}$N$_7$Se$_1$W$_{16}$Mo$_2$O$_{70}$, M_W = 4678.21 g mol^{-1}, calc (%): W 62.87, Mo 4.10, Se 1.68, H 1.70, C 3.59, N 2.09; found (%): W 57.36, Mo 3.19, Se 1.77, H 1.56, C 3.53, N 2.03. Calculated TGA water loss from 25 to 200 °C (%): calculated, 3.8; found 3.3.

Synthesis of (C$_2$H$_8$N)$_7$H$_3$[TeW$_{16}$Mo$_2$O$_{60}$]·10H$_2$O (3). Sodium tungstate dihydrate (2.5 g, 7.6 mmol), sodium tellurite (0.1 g, 0.48 mmol), and dimethylamine hydrochloride (DMA·HCl) (1.2 g, 14.7 mmol) were dissolved in 20 mL of water. Around 3 mL of {Mo$_2$} was added dropwise under stirring, and the solution pH consequently reached 1.9. The solution was heated with stirring at around 50 °C for 30 min. Upon cooling to room temperature, big dark blue block crystals were isolated from the filtrate after 1 week (Yield: 62.5% based on W). Characteristic IR bands (cm^{-1}): 3448(b), 3159(b), 3035(b), 2786(m), 2447(w), 1614(m), 1463(s), 1244(w), 1071(m), 957(s), 877(m), 713(s), 487(w). Elemental analysis for C$_{14}$H$_{79}$N$_7$Te$_1$W$_{16}$Mo$_2$O$_{70}$, M_W = 4726.85 g mol^{-1}, calc (%): W 62.23, Mo 4.06, Te 2.70, H 1.68, C 3.56, N 2.07; found (%): W 61.87, Mo 4.28, Te 2.76, H 1.77, C 3.93, N 2.26. Calculated TGA water loss from 25 to 200 °C (%): calculated, 3.8; found, 1.8.

Synthesis of (C$_2$H$_8$N)$_{11}$NaH[H$_2$P$_2$W$_{21}$Mo$_3$O$_{81}$]·15H$_2$O (4). Sodium tungstate dihydrate (1.6 g, 4.8 mmol), phosphorous acid (0.04 g, 0.48 mmol), and dimethylamine hydrochloride (DMA·HCl) (1.2 g, 14.7 mmol) were dissolved in 40 mL of water. Around 1.6 mL of {Mo$_2$} was added dropwise under stirring, and the solution pH consequently reached 3.3. The solution was heated with stirring at around 50 °C for 30 min. Upon cooling to room temperature, a dark blue powder formed and was removed by filtration. Dark blue precipitates appeared after a few days and were removed by filtration. Small dark blue star or rod-like crystals were isolated after 3 weeks. These crystals were collected by soaking the solid using filtered mother liquor to remove further blue powder (Yield: 6.3% based on W). Characteristic IR bands (cm^{-1}): 3448(b), 3140(b), 2980(s), 2787(w), 2455(w), 1614(m), 1462(s), 1381(m), 1251(m), 1149(s), 1066(m), 952(s), 731(s). Elemental analysis for C$_{22}$H$_{121}$N$_{11}$Na$_1$P$_2$W$_{21}$Mo$_3$O$_{96}$, M_W = 6309.8 g mol^{-1}, calc (%): W 61.19, Mo 4.56, P 0.98, Na 0.36, H 1.93, C 4.19, N 2.44; found (%): W 59.66, Mo 4.24, P 0.76, Na 0.79, H 1.80, C 4.06, N 2.33. Calculated TGA water loss from 25 to 200 °C (%): calculated, 4.3; found, 2.8.

Synthesis of (C$_2$H$_8$N)$_{11}$NaH$_3$[Se$_2$W$_{21}$Mo$_3$O$_{82}$]·14H$_2$O (5). Sodium tungstate dihydrate (1.36 g, 4.1 mmol), sodium selenite (0.08 g, 0.46 mmol), and dimethylamine hydrochloride (DMA·HCl) (1.2 g, 14.7 mmol) were dissolved in 20 mL of water. Around 1.5 mL of {Mo$_2$} was added dropwise under stirring, and consequently the solution pH reached 2.2. The solution was heated with stirring at around 50 °C for 30 min. Upon cooling to room temperature, a dark blue powder formed and was removed by filtration. Blue precipitates appeared constantly and were removed by filtration. Small dark blue needle-shaped crystals were isolated from the filtrate after three months. These crystals were collected by soaking the solid using filtered mother liquor to remove further blue powder (Yield: 8.0% based on W). Characteristic IR bands (cm^{-1}): 3431(b), 3159(b), 2980(m), 2879(w), 2786(w), 2436(w), 1614(m), 1462(m), 1379(m), 1253(m), 1153(m), 1070(m), 952(s), 746(s), 488(w). Elemental analysis for C$_{22}$H$_{119}$N$_{11}$Na$_1$Se$_2$W$_{21}$Mo$_3$O$_{96}$, M_W = 6403.60 g mol^{-1}, calc (%): W 60.29, Mo 4.49, Se 2.47, Na 0.36, H 1.87, C 4.12, N 2.41; found (%): W 61.87, Mo 4.48, Se 1.90, Na 0.34, H 1.71, C 4.60, N 2.40. Calculated TGA water loss from 25 to 200 °C (%): calculated, 3.9; found, 3.2.

Synthesis of (C$_2$H$_8$N)$_{10}$NaH$_3$[Te$_2$W$_{22}$Mo$_2$O$_{82}$]·14H$_2$O (6). Sodium tungstate dihydrate (7.5 g, 22.75 mmol), sodium tellurite (0.3 g, 1.35 mmol), and dimethylamine hydrochloride (DMA·HCl) (3.6 g, 44.1 mmol) were dissolved in 80 mL of water. Around 9.2 mL of {Mo$_2$} was added dropwise under stirring, and consequently the solution pH reached 2.5. The solution was heated with stirring at around 50 °C for 30 min. Upon cooling to room temperature, a dark blue powder formed and was removed by filtration. Compound **3** formed and was isolated after a few days. Afterward, blue precipitates appeared constantly and were removed by filtration. Finally, small dark blue rod-like crystals were isolated from the filtrate after four months. These crystals were collected by soaking the solid using filtered mother liquor to remove further blue powder (Yield: 7.5%

based on W). Characteristic IR bands (cm^{-1}): 3444(b), 3143(b), 2981(m), 2783(w), 2443(w), 1608(m), 1463(s), 1382(w), 1247(w), 155(w), 1082(m), 1014(m), 954(s), 858(w), 725(s), 472(w). Elemental analysis for $C_{20}H_{111}N_{10}Na_1Te_2W_{22}Mo_2O_{96}$, M_W = 6542.65 g mol^{-1}, calc (%): W 61.81, Mo 2.93, Te 3.90, Na 0.35, H 1.71, C 3.67, N 2.14; found (%): W 62.73, Mo 3.49, Te 4.82, Na 0.60, H 1.62, C 4.14, N 2.50. Calculated TGA water loss from 25 to 200 °C (%): calculated, 3.8; found, 2.5.

Synthesis of $(C_2H_8N)_{10}NaH[HPSeW_{22}Mo_2O_{81}]\cdot15H_2O$ (7). Sodium tungstate dihydrate (2.5 g, 7.6 mmol), phosphorous acid (0.02 g, 0.24 mmol), sodium selenite (0.04 g, 0.23 mmol), and dimethylamine hydrochloride (DMA·HCl) (1.2 g, 14.7 mmol) were dissolved in 20 mL of water. Around 2.6 mL of {Mo$_2$} was added dropwise under stirring, and the solution pH consequently reached 2.0. The solution was heated with stirring at around 50 °C for 30 min. Upon cooling to room temperature, a dark blue powder formed and was removed by filtration. Peanut-shaped clusters formed after a few weeks and were removed from the solution by filtration. Blue precipitates appeared constantly afterward and were also removed by filtration. After two months, blue block crystals of **7** were formed and isolated. These crystals were collected by soaking the solid using filtered mother liquor to remove further blue powder (Yield: 13.0% based on P or Se). Characteristic IR bands (cm^{-1}): 3430(b), 3032(b), 2758(w), 1694(m), 1464(s), 1246(w), 1064(m), 1016(m), 957(s), 892(w), 722(s), 550(w). Elemental analysis for $C_{20}H_{112}N_{10}Na_1Se_1P_1W_{22}Mo_2O_{96}$, M_W = 6398.59 g mol^{-1}, calc (%): W 63.21, Mo 3.00, P 0.48, Se 1.23, Na 0.36, H 1.76, C 3.75, N 2.19; found (%): W 59.12, Mo 3.63, P 0.87, Se 1.54, Na 0.25, H 1.75, C 3.87 N 2.20. Calculated TGA water loss from 25 to 200 °C (%): calculated, 4.2; found, 4.1.

Synthesis of $(C_2H_8N)_{11}NaH[HPTeW_{21}Mo_3O_{81}]\cdot15H_2O$ (8). Sodium tungstate dihydrate (2.5 g, 7.6 mmol), phosphorous acid (0.02 g, 0.24 mmol), sodium tellurite (0.05 g, 0.24 mmol), and dimethylamine hydrochloride (DMA·HCl) (1.2 g, 14.7 mmol) were dissolved in 20 mL of water. Around 2.4 mL of {Mo$_2$} was added dropwise under stirring, and the solution pH consequently reached 3.3. The solution was heated with stirring at around 50 °C for 30 min. Upon cooling to room temperature, a dark blue powder formed and was removed by filtration. Peanut-shaped clusters formed after a few weeks and were removed from the solution by filtration. Blue precipitates appeared constantly afterward and were also removed by filtration. Dark blue block crystals were isolated from the filtrate after 6 weeks. These crystals were collected by soaking the solid using filtered mother liquor to remove further blue powder (Yield: 20.0% based on P). Characteristic IR bands (cm^{-1}): 3448(b), 2958(w), 3035(b), 2872(w), 2764(m), 2420(w), 1596(m), 1463(s), 1410(w), 1379(w), 1067(m), 1016(m), 958(s), 884(s), 736(s), 563(w). Elemental analysis for $C_{20}H_{102}N_{10}Na_1P_1Te_1W_{21}Mo_3O_{91}$, M_W = 6269.25 g mol^{-1}, calc (%): W 61.58, Mo 4.59, P 0.49, Te 2.04, Na 0.37, H 1.64, C 3.83, N 2.23; found (%): W 55.1, Mo 4.19, P 0.64, Te 2.5, Na 0.29, H 1.57, C 3.70, N 2.10. Calculated TGA water loss from 25 to 200 °C (%): calculated, 4.3; found, 2.6.

Synthesis of $(C_2H_8N)_{16}[H_3P_3W_{26}Mo_4O_{102}]\cdot15H_2O$ (9). Sodium tungstate dihydrate (1.6 g, 4.8 mmol), phosphorous acid (0.04 g, 0.48 mmol), and dimethylamine hydrochloride (DMA·HCl) (1.2 g, 14.7 mmol) were dissolved in 40 mL of water. Around 1.6 mL of {Mo$_2$} was added dropwise under stirring, and the solution pH consequently reached 3.2. The solution was heated with stirring at around 65 °C for 30 min. Upon cooling to room temperature, a dark blue powder formed and was removed by filtration. Blue precipitates appeared constantly afterward and were also removed by filtration. Dark blue bar-shaped crystals of **9** mixed with **4** were found from the filtrate after two months. **Note**: Compound **9** is hard to manually separate in pure form from the mixture of **4** and **9** as they look almost the same under the microscope. Therefore, we obtained only the crystal structure of this compound and the formula was deduced based on crystal data and other new HPOMs analogues. First, the number of Mo atoms is assigned as 4 because the 4-layered cluster **10** contains 4 Mo atoms. In the same way, the overall charge is determined to be −16 considering all the Mo centers adopting +5 valence. To balance

the charge, 16 protonated dimethyl amines are proposed as the counterions. The amount of crystalline water is deduced based on other multilayered clusters (**4**−**8**) because all of them contain ∼15 crystalline waters. Therefore, the formula of **9** is reasonably determined as $(C_2H_8N)_{16}[H_3P_3W_{26}Mo_4O_{102}]\cdot15H_2O$.

Synthesis of $(C_2H_8N)_{30}NaH[Se_3W_{26}Mo_4O_{102}][Se_4W_{36}O_{124}]\cdot40H_2O$ (10). Sodium tungstate dihydrate (1.6 g, 4.8 mmol), sodium selenite (0.08 g, 0.46 mmol), and dimethylamine hydrochloride (DMA·HCl) (1.2 g, 14.7 mmol) were dissolved in 40 mL of water. Around 2.1 mL of {Mo$_2$} was added dropwise under stirring, and consequently the solution pH reached 2.4. The solution was heated with stirring at around 65 °C for 30 min. Upon cooling to room temperature, a dark blue powder formed and was removed by filtration. Precipitates formed constantly and were removed by filtration. Then, pale blue precipitates together with Trojan-horse-type $[Se_2W_{18}O_{62}(H_2O)_2]^{8-}$ appeared.[9] Dark blue needle-shaped crystals of **10** were isolated from the filtrate after two months. These crystals were collected by soaking the solid using filtered mother liquor to remove further blue powder (Yield: 11.4% based on Se). Characteristic IR bands (cm^{-1}): 3455(b), 3137(b), 2786(w), 1605(m), 1464(m), 1016(m), 951(s), 714(s), 646(s). Elemental analysis for $C_{60}H_{331}N_{30}Na_1Se_7W_{62}Mo_4O_{271}$, M_W = 18077.8 g mol^{-1}, calc (%): W 63.05, Mo 2.12, Se 3.06, Na 0.12, H 1.78, C 3.99, N 2.32; found (%): W 58.89, Mo 2.13, Se 3.31, Na 0.17, H 1.62, C 4.15, N 2.30. Calculated TGA water loss from 25 to 200 °C (%): calculated, 4.0; found, 3.7.

Synthesis of $(C_{16}H_{36}N)_5[H_3TeW_{16}Mo_2O_{60}]$ (11). Compound **3** (0.42 mmol, 2.0 g) was dissolved in 25 mL of 0.5 M HCl. Then a 15 mL solution of 5.0 g of tetrabutylammonium bromide was added under vigorous stirring. Blue powder was formed and isolated by centrifugation and collected, washed with water and ethanol, and then dried under vacuum. Recrystallization of the solid from acetonitrile with ether diffusion afforded yellow crystals of **11** (Yield: 37.10% based on compound **3**). Characteristic IR bands (cm^{-1}): 2958(m), 2872(m), 1482(s), 1464(m), 1378(m), 1151(w), 967(s), 951(s), 888(s), 771(s), 738(s). Elemental analysis for $C_{80}H_{183}N_5Te_1W_{16}Mo_2O_{60}$, M_W = 5436.4 g mol^{-1}, calc (%): W 54.10, Mo 3.53, Te 2.35, H 3.39, C 17.67, N 1.29; found (%): W 54.50, Mo 3.15, Te 3.50, H 3.34, C 17.83, N 1.30. Calculated TGA solvent loss from 25 to 250 °C (%): calculated, 0.0; found, 1.0.

■ ASSOCIATED CONTENT

Ⓢ Supporting Information

The Supporting Information is available free of charge on the ACS Publications website at DOI: 10.1021/jacs.9b04533.

Detailed synthetic procedures, crystallography, NMR spectroscopy, mass spectrometry, dielectric measurement (PDF)

Data for $(C_2H_8N)_7H_3[HPW_{16}Mo_2O_{60}]\cdot10H_2O$ (**1**) (CIF)

Data for $(C_2H_8N)_7H_3[SeW_{16}Mo_2O_{60}]\cdot10H_2O$ (**2**) (CIF)

Data for $(C_2H_8N)_7H_3[TeW_{16}Mo_2O_{60}]\cdot10H_2O$ (**3**) (CIF)

Data for $(C_2H_8N)_{11}NaH[H_2P_2W_{21}Mo_3O_{81}]\cdot15H_2O$ (**4**) (CIF)

Data for $(C_2H_8N)_{11}NaH_3[Se_2W_{21}Mo_3O_{82}]\cdot14H_2O$ (**5**) (CIF)

Data for $(C_2H_8N)_{10}NaH_3[Te_2W_{22}Mo_2O_{82}]\cdot14H_2O$ (**6**) (CIF)

Data for $(C_2H_8N)_{10}NaH[HPSeW_{22}Mo_2O_{81}]\cdot15H_2O$ (**7**) (CIF)

Data for $(C_2H_8N)_{11}NaH[HPTeW_{21}Mo_3O_{81}]\cdot15H_2O$ (**8**) (CIF)

Data for $(C_2H_8N)_{30}NaH[Se_3W_{26}Mo_4O_{102}]$-$[Se_4W_{36}O_{124}]\cdot40H_2O$ (**10**) (CIF)

Data for $(C_{16}H_{36}N)_5[H_3TeW_{16}Mo_2O_{60}]$ (**11**) (CIF)

■ AUTHOR INFORMATION

Corresponding Authors
*Deliang.Long@Glasgow.ac.uk
*Lee.Cronin@Glasgow.ac.uk

ORCID ●

De-Liang Long: 0000-0003-3241-2379
Leroy Cronin: 0000-0001-8035-5757

Notes

The authors declare no competing financial interest.

■ ACKNOWLEDGMENTS

■ REFERENCES

(1) Long, D.-L.; Tsunashima, R.; Cronin, L. Polyoxometalates: Building Blocks for Functional Nanoscale Systems. *Angew. Chem., Int. Ed.* **2010**, *49*, 1736.

(2) Mizuno, N.; Misono, M. Heterogeneous catalysis. *Chem. Rev.* **1998**, *98*, 199.

(3) Song, Y. F.; Tsunashima, R. Recent advances on polyoxometalate-based molecular and composite materials. *Chem. Soc. Rev.* **2012**, *41*, 7384.

(4) Coronado, E.; Gómez-García, C. J. Polyoxometalate-based molecular materials. *Chem. Rev.* **1998**, *98*, 273.

(5) Long, D.-L.; Burkholder, E.; Cronin, L. Polyoxometalate clusters, nanostructures and materials: From self-assembly to designer materials and devices. *Chem. Soc. Rev.* **2007**, *36*, 105.

(6) Liu, T.; Diemann, E.; Li, H.; Dress, A. W. M.; Müller, A. Self-Assembly in Aqueous Solution of Wheel-Shaped Mo154 Oxide Clusters into Vesicle. *Nature* **2003**, *426*, 59.

(7) Miras, H. N.; Cooper, G. J. T.; Long, D.-L.; Bögge, H.; Müller, A.; Streb, C.; Cronin, L. Unveiling the Transient Template in the Self-Assembly of a Molecular Oxide Nanowheel. *Science* **2010**, *327*, 72.

(8) Sadeghi, O.; Zakharov, L. N.; Nyman, M. Aqueous formation and manipulation of the iron-oxo Keggin ion. *Science* **2015**, *347*, 1359.

(9) Busche, C.; Vilà-Nadal, L.; Yan, J.; Miras, H. N.; Long, D.-L.; Georgiev, V. P.; Asenov, A.; Pedersen, R. H.; Gadegaard, N.; Mirza, M. M.; Paul, D. J.; Poblet, J. M.; Cronin, L. Design and fabrication of memory devices based on nanoscale polyoxometalate clusters. *Nature* **2014**, *515*, 545.

(10) Wang, J.-L.; Lu, Y.-R.; Li, H.-H.; Liu, J.-W.; Yu, S.-H. Large Area Co-Assembly of Nanowires for Flexible Transparent Smart Windows. *J. Am. Chem. Soc.* **2017**, *139*, 9921.

(11) Pope, M. T. *Heteropoly and Isopolyoxometalates*; Springer-Verlag: Berlin, 1983.

(12) Banerjee, A.; Bassil, B. S.; Röschenthaler, G. V.; Kortz, U. Diphosphates and diphosphonates in polyoxometalate chemistry. *Chem. Soc. Rev.* **2012**, *41*, 7590.

(13) Chen, J. J.; Symes, M. D.; Cronin, L. Highly reduced and protonated aqueous solutions of $[P_2W_{18}O_{62}]^{6-}$ for on-demand hydrogen generation and energy storage. *Nat. Chem.* **2018**, *10*, 1042.

(14) Fleming, C.; Long, D.-L.; McMillan, N.; Johnston, J.; Bovet, N.; Dhanak, V.; Gadegaard, N.; Kögerler, P.; Cronin, L.; Kadodwala, M. Reversible electron-transfer reactions within a nanoscale metal oxide cage mediated by metallic substrates. *Nat. Nanotechnol.* **2008**, *3*, 229.

(15) Long, D.-L.; Kögerler, P.; Cronin, L. Old Clusters with New Tricks: Engineering S⋯ S Interactions and Novel Physical Properties in Sulfite-Based Dawson Clusters. *Angew. Chem., Int. Ed.* **2004**, *43*, 1817.

(16) Long, D.-L.; Abbas, H.; Kögerler, P.; Cronin, L. Confined Electron-Transfer Reactions within a Molecular Metal Oxide "Trojan Horse. *Angew. Chem., Int. Ed.* **2005**, *44*, 3415.

(17) Yan, J.; Long, D.-L.; Haralampos, N. M.; Cronin, L. Cation controlled assembly and transformation of mono-and bi-sulfite templated Dawson-type polyoxotungstates. *Inorg. Chem.* **2010**, *49*, 1819.

(18) Wang, L.; Li, W.; Wu, L.; Dong, X.; Hu, H.; Xue, G.-L. A new polyanion with Dawson-like constitution: $[H_2SeW_{18}O_{60}]^{6-}$. *Inorg. Chem. Commun.* **2013**, *35*, 122.

(19) Jeannin, Y.; Martin-Frère, J. X-ray study of $(NH_4)_7[H_2AsW_{18}O_{60}]\cdot 16H_2O$: first example of a heteropolyanion containing protons and arsenic (III). *Inorg. Chem.* **1979**, *18*, 3010.

(20) Ozawa, Y.; Sasaki, Y. Synthesis and Crystal Structure of $[(CH_3)_4N]_6[H_3BiW_{18}O_{60}]$. *Chem. Lett.* **1987**, *16*, 923.

(21) Rodewald, D.; Jeannin, Y. C. R. Crystallographic and nuclear magnetic resonance study of bismuthooctadecatung-state $Na_7[H_2BiW_{18}O_{60}]\cdot 24H_2O$. *Acad. Sci. Paris Ser. II.* **1999**, *2*, 63.

(22) Zheng, Q.; Vilà-Nadal, L.; Busche, C.; Mathieson, J. S.; Long, D.-L.; Cronin, L. Following the Reaction of Heteroanions inside a {W₁₈O₅₆} Polyoxometalate Nanocage by NMR Spectroscopy and Mass Spectrometry. *Angew. Chem., Int. Ed.* **2015**, *54*, 7895.

(23) Maeda, S.; Goto, T.; Takamoto, M.; Eda, K.; Himeno, S.; Takahashi, H.; Hori, T. An Approach to the Synthesis of Polyoxometalate Encapsulating Different Kinds of Oxoanions as Heteroions: Bisphosphitopyrophosphatotriacontamolybdate $[(HPO_3)_2(P_2O_7)Mo_{30}O_{90}]^{8-}$. *Inorg. Chem.* **2008**, *47*, 11197.

(24) Eda, K.; Den, K.; Himeno, S. A new class of 30-tungsto polyoxometalates: Preparation, structure, and electrochemical properties of bispyrophosphatotriacontatungstate $[(P_2O_7)_2W_{30}O_{90}]^{8-}$. *Inorg. Chim. Acta* **2012**, *382*, 182.

(25) Kortz, U. Polyoxometalate-Diphosphate Complexes. 5.1 Cigar-Shaped 30-Molybdobispyrophosphate: Structure of $(N(C_4H_9)_4)_2H_9[\{(P_2O_7)Mo_{15}O_{45}\}_2][PMo_{12}O_{40}]$. *Inorg. Chem.* **2000**, *39*, 623.

(26) Eda, K.; Maeda, S.; Himeno, S.; Hori, T. A new class of 30-molybdo complexes: Formation, structure and electrochemical properties of bisselenitopyrophosphatotriacontamolybdate, $[(SeO_3)_2(P_2O_7)Mo_{30}O_{90}]^{8-}$, and bispyrophosphatotriacontamolybdate, $[(P_2O_7)_2Mo_{30}O_{90}]^{8-}$. *Polyhedron* **2009**, *28*, 4032.

(27) Müller, A.; Gouzerh, P. From linking of metal-oxide building blocks in a dynamic library to giant clusters with unique properties and towards adaptive chemistry. *Chem. Soc. Rev.* **2012**, *41*, 7431.

(28) Müller, A.; Krickemeyer, E.; Meyer, J.; Bögge, H.; Peters, F.; Plass, W.; Diemann, E.; Dillinger, S.; Nonnenbruch, F.; Randerath, M.; Menke, C. $[Mo_{154}(NO)_{14}O_{420}(OH)_{28}(H_2O)_{70}]^{(25\pm5)-}$: A Water-Soluble Big Wheel with More than 700 Atoms and a Relative Molecular Mass of About 24000. *Angew. Chem., Int. Ed. Engl.* **1995**, *34*, 2122.

(29) Müller, A.; Krickemeyer, E.; Bögge, H.; Schmidtmann, M.; Beugholt, C.; Kögerler, P.; Lu, C. Formation of a Ring-Shaped Reduced "Metal Oxide" with the Simple Composition $[(MoO_3)_{176}(H_2O)_{80}H_{32}]$. *Angew. Chem., Int. Ed.* **1998**, *37*, 1220.

(30) Müller, A.; Beckmann, E.; Bögge, H.; Schmidtmann, M.; Dress, A. Inorganic Chemistry Goes Protein Size: A Mo₃₆₈ Nano-Hedgehog Initiating Nanochemistry by Symmetry Breaking. *Angew. Chem., Int. Ed.* **2002**, *41*, 1162.

(31) (a) Müller, A.; Kögerler, P.; Kuhlmann, C. A variety of combinatorially linkable units as disposition: from a giant icosahedral Keplerate to multi-functional metal—oxide based network structures. *Chem. Commun.* **1999**, *15*, 1347.

(32) Müller, A.; Krickemeyer, E.; Bögge, H.; Schmidtmann, M.; Peters, F. Organizational forms of matter: an inorganic super fullerene and keplerate based on molybdenum oxide. *Angew. Chem., Int. Ed.* **1998**, *37*, 3359.

(33) Schäffer, C.; Merca, A.; Bögge, H.; Todea, A. M.; Kistler, M. L.; Liu, T.; Thouvenot, R.; Gouzerh, P.; Müller, A. Unprecedented and Differently Applicable Pentagonal Units in a Dynamic Library: A Keplerate of the Type $\{(W)W_5\}_{12}\{Mo_2\}_{30}$. *Angew. Chem., Int. Ed.* **2009**, *48*, 149.

(34) Schaffer, C.; Todea, A. M.; Bögge, H.; Petina, O. A.; Rehder, D.; Haupt, E. T. K.; Müller, A. Hydrophobic Interactions and Clustering in a Porous Capsule: Option to Remove Hydrophobic Materials from Water. *Chem. - Eur. J.* **2011**, *17*, 9634.

(35) Dolbecq, A.; Compain, J. D.; Mialane, P.; Marrot, J.; Sécheresse, F.; Keita, B.; Holzle, L. R. B.; Miserque, F.; Nadjo, L. Hexa-and Dodecanuclear Polyoxomolybdate Cyclic Compounds: Application toward the Facile Synthesis of Nanoparticles and Film Electrodeposition. *Chem. - Eur. J.* **2009**, *15*, 733.

(36) Zheng, Q.; Vilà-Nadal, L.; Lang, Z.; Chen, J.-J.; Long, D.-L.; Mathieson, J. S.; Poblet, J. M.; Cronin, L. Self-sorting of heteroanions in the assembly of cross-shaped polyoxometalate clusters. *J. Am. Chem. Soc.* **2018**, *140*, 2595.

(37) Gao, J.; Yan, J.; Beeg, S.; Long, D.-L.; Cronin, L. Assembly of molecular "Layered" heteropolyoxometalate architectures. *Angew. Chem., Int. Ed.* **2012**, *51*, 3373.

(38) Potapova, L. V.; Karpukhina, T. A.; Kazanskii, L. P.; Spitsyn, V. I. ESR spectra of molybdenum(V) in $PMo_xW_{12-x}O_{40}{}^{n-}$ heteropolyanions. *Bull. Acad. Sci. USSR, Div. Chem. Sci.* **1979**, *28*, 674−678.

(39) So, H.; Pope, M. T. Origin of some charge-transfer spectra. Oxo compounds of vanadium, molybdenum, tungsten, and niobium including heteropoly anions and heteropoly blues. *Inorg. Chem.* **1972**, *11*, 1441.

(40) Martin-Sabi, M.; Soriano-Lopez, J.; Winter, R. S.; Chen, J.-J.; Vilà-Nadal, L.; Long, D.-L.; Galan-Mascaros, J. R.; Cronin, L. Redox tuning the Weakley-type polyoxometalate archetype for the oxygen evolution reaction. *Nat. Catal.* **2018**, *1*, 208.

(41) Nakamura, I.; Tsunashima, R.; Nishihara, S.; Inoue, K.; Akutagawa, T. A dielectric anomaly observed for doubly reduced mixed-valence polyoxometalate. *Chem. Commun.* **2017**, *53*, 6824.

(42) Meng, X.; Wang, H.-N.; Song, S.-Y.; Zhang, H.-J. Proton-conducting crystalline porous materials. *Chem. Soc. Rev.* **2017**, *46*, 464.

(43) Sheldrick, G. Phase annealing in SHELX-90: direct methods for larger structures. *Acta Crystallogr., Sect. A: Found. Crystallogr.* **1990**, *A46*, 467−473.

(44) Sheldrick, G. A short history of SHELX. *Acta Crystallogr., Sect. A: Found. Crystallogr.* **2008**, *A64*, 112−122.

(45) Farrugia, L. WinGX suite for small-molecule single-crystal crystallography. *J. Appl. Crystallogr.* **1999**, *32*, 837−838.

(46) Clark, R. C.; Reid, J. S. The analytical calculation of absorption in multifaceted crystals. *Acta Crystallogr., Sect. A: Found. Crystallogr.* **1995**, *A51*, 887−897.